Journal of Quantitative Spectroscopy & Radiative Transfer 186 (2017) 3–16

Contents lists available at ScienceDirect

Journal of Quantitative Spectroscopy & Radiative Transfer

journal homepage: www.elsevier.com/locate/jqsrt

The Atmospheric Chemistry Experiment (ACE)

P.F. Bernath [a,b]

[a] Department of Chemistry and Biochemistry, Old Dominion University, Norfolk, VA 23529, USA
[b] Department of Chemistry, University of Waterloo, Waterloo, Ontario, Canada N2L 3G1

ARTICLE INFO

Article history:
Received 14 January 2016
Received in revised form
8 April 2016
Accepted 8 April 2016
Available online 16 April 2016

Keywords:
Satellite remote sensing
Fourier transform spectroscopy
Space science
Atmospheric science
Solar occultation

ABSTRACT

The Atmospheric Chemistry Experiment (ACE), also called SCISAT, is a Canadian-led small satellite mission for remote sensing of the Earth's atmosphere. ACE was launched into a low Earth circular orbit by NASA on August 12, 2003 and it continues to function nominally. The ACE instruments are a high spectral resolution (0.02 cm^{-1}) Fourier Transform Spectrometer (FTS) operating from 2.2 to 13.3 μm (750–4400 cm^{-1}), a spectrophotometer known as Measurement of Aerosol Extinction in the Stratosphere and Troposphere Retrieved by Occultation (MAESTRO) with wavelength coverage of 285–1020 nm and two filtered detector arrays to image the Sun at 0.525 and 1.02 μm. ACE operates in solar occultation mode to provide altitude profiles of temperature, pressure, atmospheric extinction and the volume mixing ratios (VMRs) for several dozen molecules and related isotopologues. This paper presents a mission overview and a summary of selected scientific results.

Contents

E-mail address: pbernath@odu.edu

http://dx.doi.org/10.1016/j.jqsrt.2016.04.006
0022-4073/

1. Introduction

Satellite instruments such as the ACE-FTS provide a global view of the state of the Earth's atmosphere in a way that is not possible from the ground, aircraft or balloon-borne platforms. The original primary ACE goal [1] was to improve our understanding of "the chemical and dynamical processes that control the distribution of ozone in the stratosphere and upper troposphere, particularly in the Arctic". Stratospheric ozone is important because it protects us from deleterious ultraviolet radiation and in the upper troposphere ozone is a greenhouse gas that contributes to climate change. Because of ACE's longevity (more than 12.5 years in orbit), changes in atmospheric composition can be measured: e.g., CO_2 increases in the upper atmosphere [2] that are associated with climate change and decreases in halogen-containing gases [3] due to the beneficial effects of the Montreal Protocol banning substances that deplete the stratospheric ozone layer. ACE also can measure a wide variety of organic molecules and nitrogen oxides in the upper troposphere that are responsible for air pollution. Process studies with ACE data have discovered the direct injection of pollution into the stratosphere by the Asian monsoon [4] and the effects of the Arctic and Antarctic oscillations on the variability of upper tropospheric water vapor in polar regions [5].

The primary instrument [6] on ACE is a high resolution ($0.02\ cm^{-1}$) infrared Fourier transform spectrometer (ACE-FTS), operating from 750 to $4400\ cm^{-1}$, used to determine the vertical profiles of trace gas volume mixing ratios (VMRs) and temperature. During sunrise and sunset, the FTS measures sequences of atmospheric absorption spectra in the limb viewing geometry (Fig. 1) with different slant paths and tangent heights; when these spectra are analyzed on the ground, the results are converted into vertical profiles of numerous atmospheric constituents. The vertical resolution is about 3 km from an altitude of 5 km (or the cloud tops) up to 150 km. Aerosols and clouds are being monitored using the extinction of solar radiation as measured by two filtered imagers and with an instrument called Measurement of Aerosol Extinction in the Stratosphere and Troposphere Retrieved by Occultation (MAESTRO). MAESTRO is a dual optical spectrophotometer [7,8] that covers the 285–1020 nm spectral region with a spectral resolution of about 2 nm. It has a vertical resolution of about 1 km and measures primarily ozone, nitrogen dioxide and aerosol/cloud extinction.

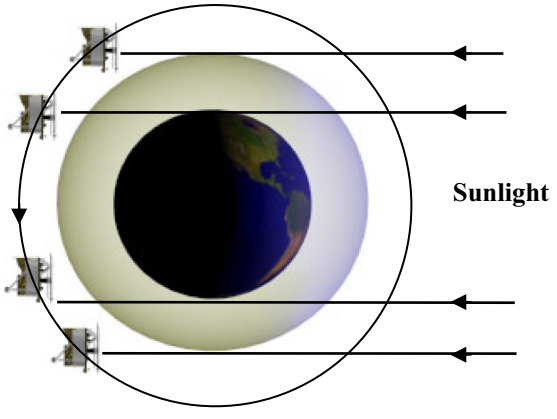

Fig. 1. Solar occultation geometry showing sunrise and sunset [28].

In general, limb sounders like the ACE-FTS offer high vertical resolution (~3 km), but low horizontal resolution (~300 km) in the limb direction. In contrast, nadir sounders usually have poor vertical resolution (often retrieving only the total column density), but high spatial resolution (e.g., 13 km by 24 km for OMI, Ozone Monitoring Instrument, on Aura [9]). Some instruments such as Tropospheric Emission Spectrometer (TES) on Aura [10] and SCanning Imaging Absorption spectroMeter for Atmospheric CHartographY (SCIAMACHY) on Envisat [11] are capable of both limb and nadir observations, although TES now operates only in nadir mode. The loss of Envisat in 2012 after a 10-year mission was very unfortunate; it had three instruments, Michelson Interferometer for Passive Atmospheric Sounding (MIPAS) [12], Global Ozone Monitoring by Occultation of Stars (GOMOS) [13] and SCIAMACHY [11] that made limb measurements.

There are currently six limb sounders making observations in addition to ACE-FTS and MAESTRO: Submillimeterwave Radiometer (SMR) [14] and Optical Spectrograph and Infrared Imaging System (OSIRIS) [15] on Odin, Sounding of the Atmosphere using Broadband Emission Radiometry (SABER) [16] on Thermosphere Ionosphere Mesosphere Energetics Dynamics (TIMED), Solar Occultation For Ice Experiment (SOFIE) [17] on Aeronomy of Ice in the Mesosphere (AIM), Microwave Limb Sounder (MLS) [18] on Aura, and Ozone Mapping Profiler Suite-Limb (OMPS-L) [19] on National Polar-orbiting Operational Environmental Satellite System Preparatory Project (Suomi-NPP). SMR and MLS measure pure rotational emission of atmospheric molecules in the limb direction. OSIRIS and OMPS-L measure limb-scattered sunlight in the UV/visible/Near Infrared spectral regions. SABER is a broadband limb-scanning infrared emission radiometer and SOFIE, like ACE-FTS, is an infrared solar occultation instrument but uses filters like SABER, rather than a spectrometer. Except for OMPS-L, these instrument are all well past their design lifetimes, which for example was just 2 years for ACE.

The rapid global coverage possible with nadir sounders is very attractive for many applications such as numerical weather forecasting; for example, Infrared Atmospheric Sounding Interferometer (IASI) [20] on MetOp-A offers global

coverage twice per day with a 12×12 km^2 nadir footprint. A number of nadir sounders are therefore planned including the UV/visible TEMPO spectrometer [21] on a geostationary platform and TROPOspheric Monitoring Instrument (TROPOMI) instrument [22] on the Sentinal-5 Precursor satellite. In contrast, the future is more limited for limb sounders with only two instruments planned: Stratospheric Aerosol and Gas Experiment (SAGE-III) on the International Space Station (ISS) with a 2016 launch and OMPS-L on Joint Polar Satellite System (JPSS-2) with a 2022 launch date.

2. ACE history

The ACE mission was inspired by the successful (but now retired) Atmospheric Trace MOlecule Spectroscopy (ATMOS) instrument that flew four times (1985, 1992, 1993, and 1994) on the Space Shuttle [23]. The ACE-FTS instrument has been miniaturized by nearly a factor of 10 in mass, power, and volume as compared to ATMOS, although ATMOS had twice the resolving power. The ACE mission was augmented by the two imagers and the MAESTRO spectrophotometer as compared to ATMOS. The imagers and MAESTRO give high signal-to-noise ratio (SNR) measurements of atmospheric extinction and lead to SAGE-like aerosol and cloud data products [24].

The ACE mission proposal was written in the fall of 1997 in Brussels, Belgium and included contributions from Belgium (e.g., CMOS imaging detectors) and USA (e.g., software from NASA-Langley). The proposal was submitted to the Canadian Space Agency (CSA) in January 1998 and was selected in November 1998 after a six-month Phase A study. The original proposal did not include MAESTRO, which was added to the payload in 1999 in order to extend the wavelength coverage and improve the aerosol data products. The instruments and spacecraft were constructed in Canada with CSA acting as the prime contractor. The ACE-FTS, including the imagers, was built by ABB-Bomem (now just ABB) in Quebec City and the satellite bus (i.e., the spacecraft apart from the instruments) was made by Bristol Aerospace (part of Magellan Aerospace) in Winnipeg. MAESTRO, with T. McElroy as the instrument principal investigator, was designed and built mainly at Environment Canada in Toronto with EMS Technologies in Ottawa (now COM DEV International) supplying some of the flight hardware.

After completion the instruments and bus were tested by the manufacturers to ensure compliance with engineering requirements. MAESTRO and FTS were then shipped to the Instrument Calibration Facility at the University of Toronto and were tested together under simulated on-orbit conditions during March 2003. The instrument performance was very good and final integration with the bus was then carried out at CSA's David Florida Laboratory near Ottawa. ACE was launched by NASA on August 12, 2003 from Vandenburg Air Force Base in California using a three-stage Pegasus XL rocket supplied by Orbital Sciences (now Orbital ATK). The launch of the Pegasus rocket from the bottom of an adapted jumbo jet flying over the Pacific Ocean was successful. The time between proposal and launch (5 years) is considered to be relatively short compared to other space projects.

Satellite commissioning on orbit lasted until February 2004, when the first science data were collected. The ACE mission was designed for a two-year lifetime and is now in its thirteenth year with only minor degradation in performance.

3. ACE instruments

3.1. FTS

The main instrument on SCISAT is a Michelson interferometer (ACE-FTS) [6] designed and built specifically for the project (Fig. 2). The optical design (Fig. 3) uses cube corner retroreflectors driven by a double pendulum mechanism (Fig. 1, left panel) to change the optical path difference. It weighs about 41 kg and has an average power consumption of 37 W, including the two imagers. The interferometer records doubled-side interferograms with a maximum optical path difference of ± 25 cm, corresponding to a spectral resolution of 0.025 cm^{-1} (full-width at half maximum of the instrument sinc function lineshape) or with the usually quoted instrument sampling of 0.02 cm^{-1} (0.5/maximum optical path difference).

In Fig. 3 the light enters from the lower right with a suntracker mirror (also Fig. 1, right panel) controlled by a quad cell. The quad cell points the suntracker mirror at the center of radiance of the Sun to better than 0.01 mrad using 4 photodiodes and a 1.55 μm optical filter. A 5:1 magnification telescope changes the external circular field of view of 1.25 mrad to 6.25 mrad inside the interferometer. From the ACE orbit altitude of 650 km, the limb of the Earth is about 3000 km away from the spacecraft so the field of view is 3–4 km on the limb, compared to the Sun diameter of 9 mrad or about 27 km projected on the limb.

The collimated infrared radiation is split by the ZnSe beamsplitter plate and double-passed through the interferometer by retroreflection from the end mirror (Fig. 3). This design makes the interferometer compact with a physical motion of only ± 3.125 cm of the cube-corners resulting in an 8-times larger optical path difference. Moreover, the instrument is “permanently aligned”, i.e., compensated for tilt and shear of the fixed and moving optics. The two arms of the interferometer (Fig. 2, left side) are driven by a voice coil and rotate on a central flex pivot to produce the optical path difference. After recombination on the beamsplitter, the radiation is sent through a hole in the end mirror to the detector assembly (Fig. 2, just on top of the optics box) where a dichroic optic divides the beam for the photovoltaic InSb and MCT (mercury cadmium telluride) detectors. The detectors are cooled to about 80 K by the two-stage passive cooler built by Ball Aerospace (Fig. 2, on the top). The cooler works by sending the thermal radiation emitted by the detector assembly to deep space.

The motion of the rotary arm and the sampling of the interferogram are controlled by the interference signal created with a distributed-feedback (DFB) diode laser working at 1.55 μm. The laser beam is inserted into the interferometer and extracted using prisms (Fig. 3), and detected with a photodiode assembly. The InSb and MCT detector signals are each digitized with two 12-bit ADCs (analog-to-digital converters), offset in gain by a factor of

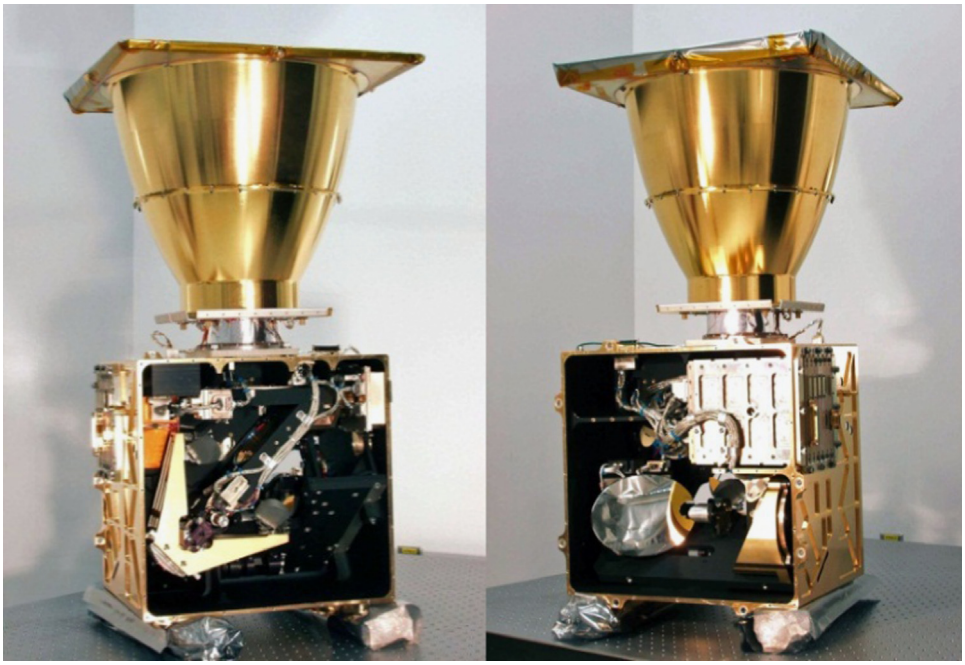

Fig. 2. ACE-FTS from the interferometer side (left panel) and from the input telescope side (right panel) [6]. The instrument electronics box is also visible in the right panel and the detector/passive cooler assembly is on top.

64 to increase the dynamic range. The low gain ADC records about 3000 data points near the zero-path difference. These digitized interferograms and housekeeping data (such as temperatures and detector DC signal levels) are sent to the satellite bus, where they are packetized and sent to the ground by an S-band microwave link. Double-sided interferograms are Fourier transformed on the ground to obtain the desired atmospheric spectra.

The main advantage of using double-sided interferograms (apart from the improved phase correction in the Fourier transformation) is that the effects on the spectra of the apparent motion of the Sun are canceled (to first order). The ACE-FTS tracks continuously (not step-and-stare) as the Sun rises or sets so the altitudes sampled are changing during a 2 s scan. Using doubled-sided interferograms corrects exactly for all linear changes in the signal due to the changing field-of-view. For some molecules such as water vapor in the troposphere that changes very rapidly with altitude, the retrieved VMR is still affected by the motion of the scene. The time resolution (and vertical sampling) could be improved by a factor of two by using single-sided interferograms, but only at the expense of degraded accuracy in the VMR retrievals.

For a sunset occultation, the measurement sequence starts by pointing the suntracker to deep space to record a set of 16 instrument self-emission spectra. The deep space spectra are followed by a set of high Sun reference spectra, and then a sequence of atmospheric spectra starting at 150 km tangent altitude are obtained at a rate of one scan every 2 s as the Sun sets. Spectra are recorded in both scan directions, and the "forward" and "reverse" scans are processed separately. The measurement sequence is over when the signal levels of the quad cell detectors fall below a preset value and the suntracker ceases solar tracking, causing the Sun to drift out of the field of view. This happens either when a cloud blocks the Sun or at about 5 km of altitude, whichever comes first. For sunrise occultations the measurement order is reversed.

Notice that the ACE-FTS vertical *resolution* is set by the input field of view of 1.25 mrad (3–4 km) but the vertical measurement *sampling* is determined by atmospheric refraction, the beta angle (defined as the angle between the orbit plane and the Earth-Sun vector) and the constant 2 s time needed to record a spectrum. As viewed from the satellite, when the beta angle is small then the Sun sets nearly vertically and the altitude sampling is about 6 km for high Sun observations; when the beta angle is large (e.g., 55°) then the Sun sets obliquely and the vertical sampling is about 2 km. Atmospheric refraction affects the solar rays entering the instrument below about 50 km in tangent altitude and compresses the sampling at low altitudes.

The ACE-FTS design is very successful resulting in a reliable space instrument with a long lifetime and unique performance. It has both high spectral resolution and a high continuum signal-to-noise ratio (typically more than 300 over most of the wavenumber range) which allows many minor atmospheric species to be measured relatively free from interference from other atmospheric molecules. The ACE design served as the basis for the GOSAT interferometer [25], a nadir sounder that is measuring carbon dioxide and methane total columns.

3.2. Imagers

The ACE-FTS also includes two filtered solar imagers (Fig. 3) [26,27] to look at clouds in the field of view (FOV) and to measure atmospheric extinction. The visible imager

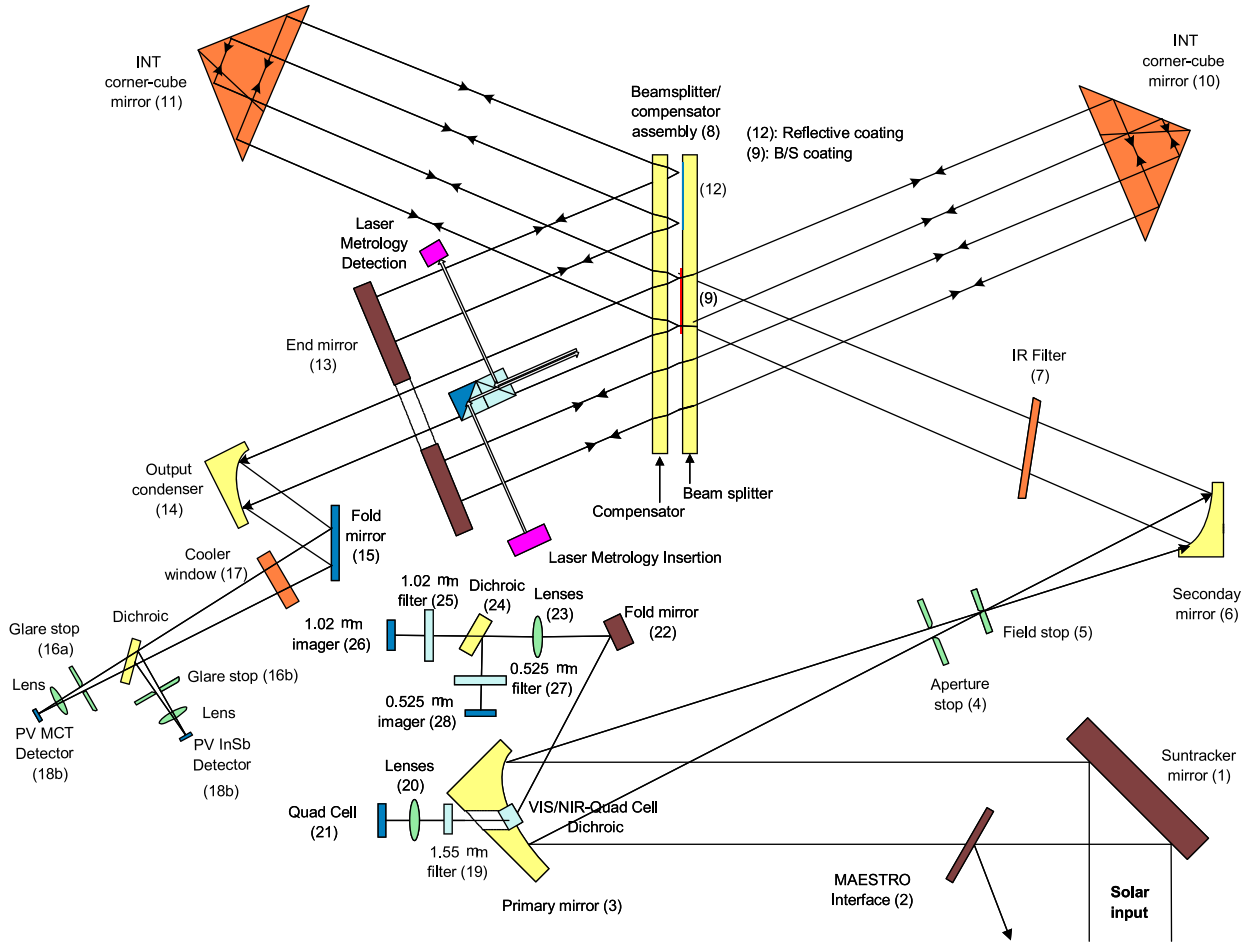

Fig. 3. Schematic ACE-FTS optical layout [6].

and near infrared imagers have filters centered at 0.525 and 1.02 μm, respectively, chosen to match two of the seven wavelengths monitored by the SAGE II satellite instrument [24]. The detectors in the imagers are (effectively) 128×128 complementary metal oxide semiconductor (CMOS) active pixel sensors made by Fill Factory (now part of ON Semiconductor) of Mechelen, Belgium. The total FOV of the imagers is 30 mrad, to be compared to the 9 mrad angular diameter of the Sun, and each pixel subtends 0.23 mrad (or 0.7 km projected on the limb). The images are summed and then saved every 0.25 s. Each final image has a signal-to-noise ratio greater than 1000 for the unattenuated high Sun, but the main image suffers from overlap by weak secondary images from optical filters that were not tipped far enough off the optical axis. The imagers are not used directly for ACE-FTS data processing, but provide auxiliary information used to verify the presence of clouds in the field-of-view.

3.3. *MAESTRO*

MAESTRO [7,8] is a small (about 8 kg) dual spectrophotometer (Fig. 4). The use of two spectrographs (285–550 nm, 525–1020 nm) reduces stray light and permits simultaneous measurements of the two bands with a spectral resolution of 1–2 nm, depending on wavelength. The input port views sunlight from a pick-off mirror (Fig. 3) from the suntracker inside the ACE-FTS and the light is diffracted with a simple concave grating with no moving parts (Fig. 4). The entrance slit is held horizontal with respect to the horizon during sunrise and sunset. The detectors are 1024 element linear EG&G Reticon photodiode arrays. A complicated detector read-out strategy is used to increase the effective dynamic range and the resulting signal-to-noise ratio is more than 1000 for high Sun spectra. MAESTRO has two backscatter ports (Fig. 4) to view the sun-lit Earth between occultations, but this mode has not produced useful data. MAESTRO has been affected by the gradual build-up of contamination of unknown origin and by 2015, no light with a wavelength shorter than about 500 nm is transmitted through the instrument. It is likely these contaminants are organic in nature because the ACE-FTS has measured the spectra of organic molecules in its optical path. These organic contaminants have characteristic infrared absorption features assignable for example to C–H stretching modes. The organic contaminants degrade the signal-to-noise ratio of the ACE-FTS atmospheric transmission spectra, but their effect is relatively isolated and not as severe as for MAESTRO.

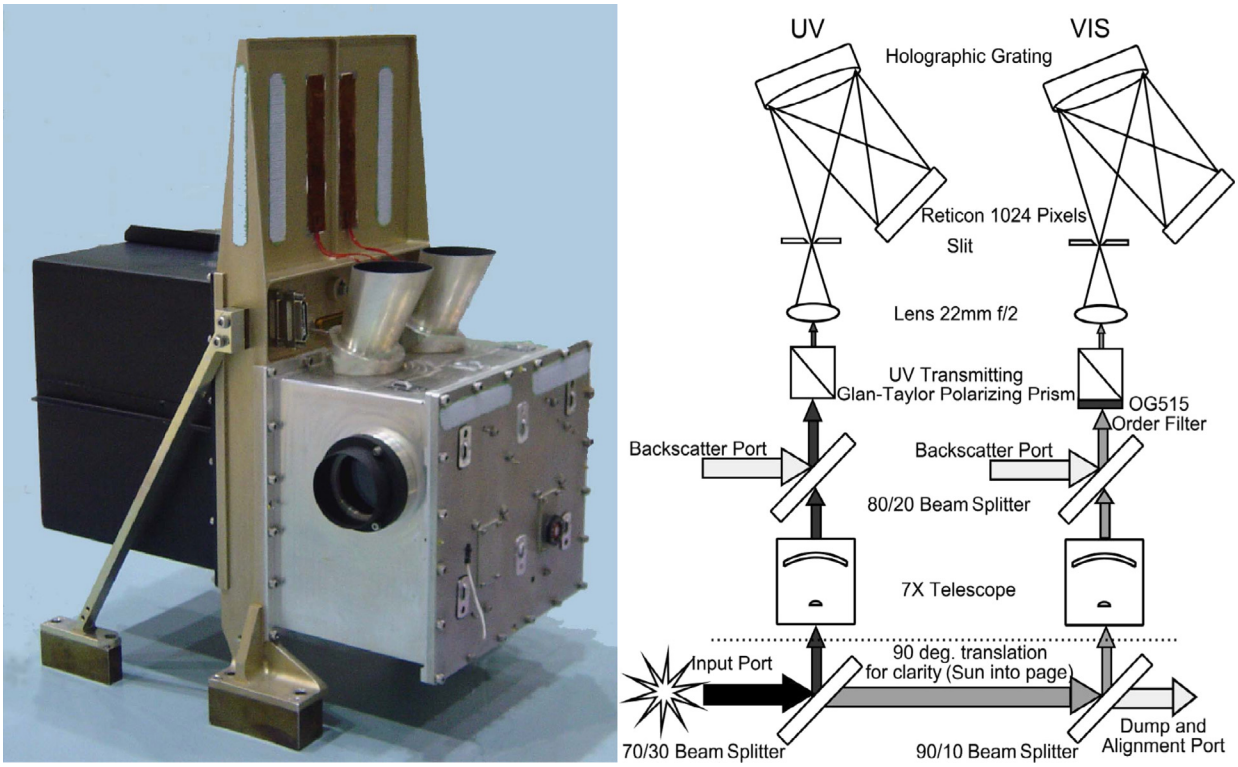

Fig. 4. MAESTRO instrument (left panel) showing the input port (black on the right) and radiator on top [8]. The right panel is a schematic of the MAESTRO optics.

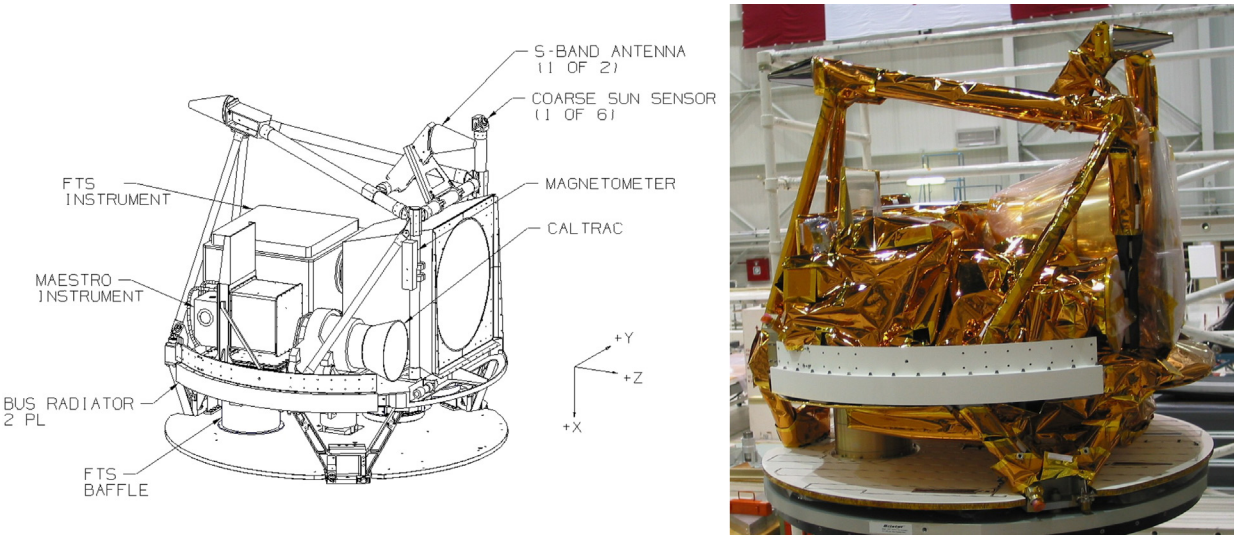

Fig. 5. SCISAT schematic drawing (left panel) and fully assembled spacecraft on the right [28].

4. Spacecraft

SCISAT [28] is a small science satellite with a mass of 152 kg, a diameter of 112 cm and generates 175 W of peak power from solar cells (Fig. 5). Because of cost constraints, a simple “single string” design architecture was used with very little redundancy. The main spacecraft structure (Fig. 5) is a plate to which ACE-FTS, MAESTRO and the CALTRAC star tracker (from EMS, now MDA Montreal) are mounted. The CALTRAC was added to control the spacecraft roll to help orient the MAESTRO slit, but it failed in 2015 with no effect on instrument performance. The solar cells are attached to a second plate, at the bottom of the images in Fig. 5, fastened by struts to the main plate. The suntracker inside the FTS looks through a baffle from the main plate to a hole in the bottom plate. The remaining structural element is a frame

that supports the two S-band microwave antennas that communicate with the ground stations and supports some of the attitude control elements.

SCISAT is a 3-axis stabilized, sun-pointing satellite with the bottom plate always facing the direction of the Sun ($+X$) even during the night. The FTS radiator is always pointing ($+Z$) towards deep space to cool the infrared detectors. The attitude control system is based on six coarse Sun sensors mounted around the spacecraft, a fine Sun sensor mounted on the main plate viewing the Sun through an aperture in the bottom plate and a magnetometer mounted on the frame. The attitude is adjusted with 3 magnetic torque rods perpendicular to each other and a rotating momentum wheel which is along the sun-pointing $+X$ direction. The orientation of the satellite is measured by the Sun sensors, and the strength and direction of the Earth's magnetic field measured by the 3-axis magnetometer. The spacecraft attitude is changed slowly by energizing the magnetic torque rods which interact with the Earth's magnetic field and by changing the rotation rate of the momentum wheel to rapidly adjust the spacecraft roll (360° per orbit) as needed to keep the FTS passive cooler pointing away from the Earth. Even without the star tracker, the attitude control system (based mainly on the magnetometer and Sun sensors) is able to orient the MAESTRO slit to better than 1° during both sunrise and sunset.

Thermal control of the spacecraft is very important mainly because electronics and optical systems are designed to work at room temperature. The spacecraft therefore regulates temperature with radiators (Fig. 5) plus heaters in various locations and is covered almost entirely in multilayer insulation (MLI) blankets (Fig. 5, right panel, gold-colored metalized plastic). Spacecraft power is obtained from a battery charged by the solar cells.

The spacecraft computer controls all operations including attitude control, instrument control, command and telemetry processing, science data storage, power management, thermal control and housekeeping. The satellite operates from a list of timed commands that are regularly up-loaded from the main ground station at CSA headquarters in St. Hubert, Quebec. SCISAT has been very successful with very few anomalies in more than 65,000 orbits.

5. Launch and orbit

ACE was launched on August 12, 2003 into a nearly circular orbit with an altitude of 650 km and the orbit plane is inclined by 73.9° to the equator. The inclination angle was selected so that the latitude (but not the longitude) of the spacecraft (and its observations) repeats annually. The satellite is in a precessing orbit and the latitudes of the occultations for one year are displayed in Fig. 6. The beta angle is also plotted and for two high beta periods in December and June there are no occultations because the orbit plane is nearly perpendicular to the Earth-Sun vector. Notice that the sunrises and sunsets are usually in opposite hemispheres, but they switch hemispheres 6 times per year. The orbital period is 97.6 min so there are about 30 occultations per day (15 sunrises and 15 sunsets) and are distributed approximately along two longitude circles about the Earth. Each of the 15 sunrises or sunsets is spaced by about 24° of longitude equivalent to about 2600 km near the equator.

SCISAT has no fuel so cannot adjust its orbit, which is sinking at an average of about 1 km/year because of atmospheric drag. The latitude sampling as shown in Fig. 6 for 2015 has also drifted by about 1 week over the course of the mission.

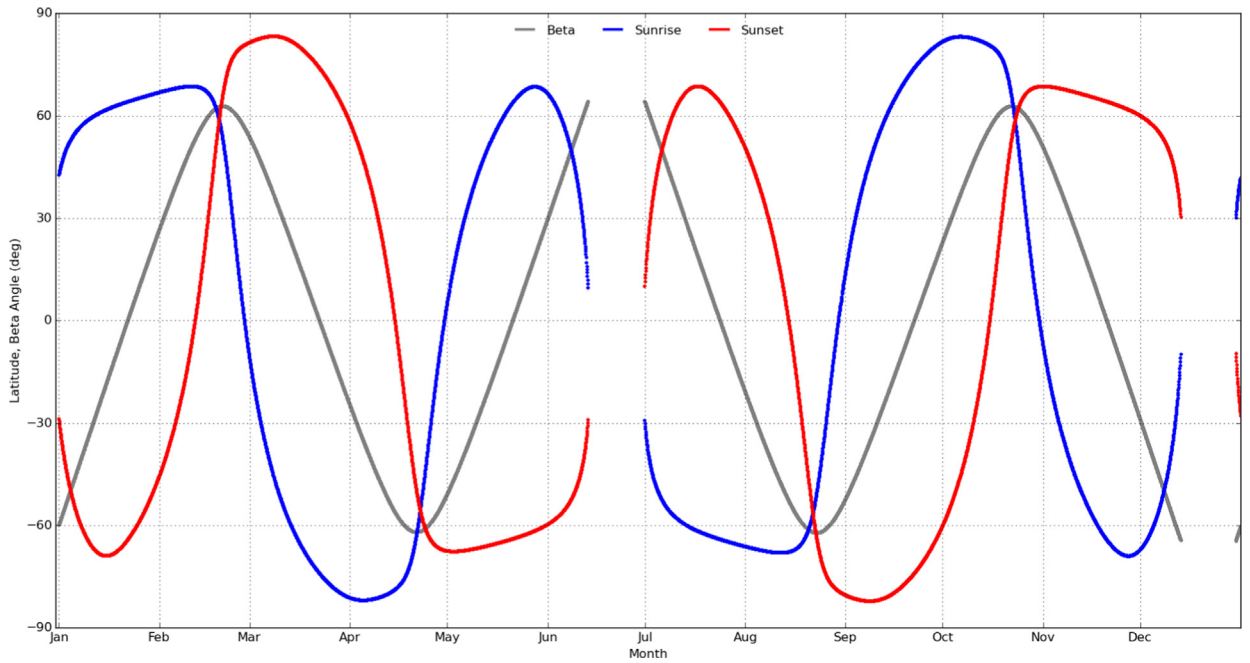

Fig. 6. The latitude of ACE occultations for 1 year (2015) and the beta angle of the orbit.

6. Ground segment

The raw ACE data are down-linked using 4 main ground stations: the CSA stations in St. Hubert, Quebec and Saskatoon, Saskatchewan, the NASA-supported Alaska Satellite Facility (ASF) in Fairbanks, Alaska and the European Space Agency's (ESA's) Kiruna station in Sweden. ACE is an ESA "third-party" mission. On-board data storage is 1.5 GB and the maximum raw data volume is about 2 GB per day, with most of the possible data down-linked every day. The data are all transferred by internet to the Mission Operations Center (MOC) in St. Hubert and then on to the Science Operations Center (SOC) at the University of Waterloo, Waterloo, Ontario. The MOC operates the satellite and uplinks the list of commands needed to run the satellite. The SOC prepares a weekly schedule of the desired occultations subject to various constraints including the amount downlink time available and the MOC translates this list into a timeline of satellite commands. The SOC archives the data and prepares data products for distribution.

The raw data from the MOC are Level 0; Level 1 data are calibrated atmospheric transmission spectra for ACE and MAESTRO, and solar images from the imagers; Level 2 data are altitude profiles of VMRs of atmospheric molecules or of atmospheric extinction. In the case of ACE-FTS the Level 0 to 1 step uses software provided by the instrument contractor, ABB, to make various corrections such as for instrument self-emission, Fourier transforms interferograms into spectra and then ratios atmospheric spectra with the average of high Sun exoatmospheric spectra to compute atmospheric transmission spectra [6]. The Level 1 to 2 step uses software written primarily by C. Boone (University of Waterloo) at the SOC [29,30]. For MAESTRO, software is primarily from T. McElroy (York University) [7,8] and is run at the University of Toronto, with final results transferred to the SOC for distribution. The imager software runs at the SOC and was mainly the responsibility of K. Gilbert. All Level 2 data are freely available upon request.

7. Data analysis

7.1. FTS processing

The Level 1 ACE-FTS atmospheric transmission spectra are of high quality (Fig. 7), although some traces of residual solar lines (mainly CO) remain. The first step in the analysis [29,30] is to retrieve the atmospheric profile of temperature and pressure as well as the tangent altitudes using CO_2 absorption lines, followed by VMR retrievals of atmospheric constituents in a second step, holding temperature and pressure constant. Selected microwindows (i.e., short segments 0.3–1 cm^{-1} wide for lines and longer segments for cross sections) in these raw spectra are used without apodization. The retrievals use a global fit approach [31], adjusting values at all altitudes simultaneously using the Levenburg-Marquardt non-linear least-squares method. The current FTS processing version is 3.5.

The atmosphere is modeled as 150 spherical shells, each 1 km thick. The FTS forward model calculates the atmospheric transmission (Fig. 1) for a refracted ray using the Beer-Lambert law [32] and spectroscopic line parameters and absorption cross sections from the HITRAN 2004 [33] database plus some updates. Voigt lineshape functions are used although some non-Voigt effects can be noted in the observed minus calculated spectral residuals. The semi-empirical FTS instrument lineshape function (ILS) has been carefully adjusted using isolated high altitude CO_2 lines. As

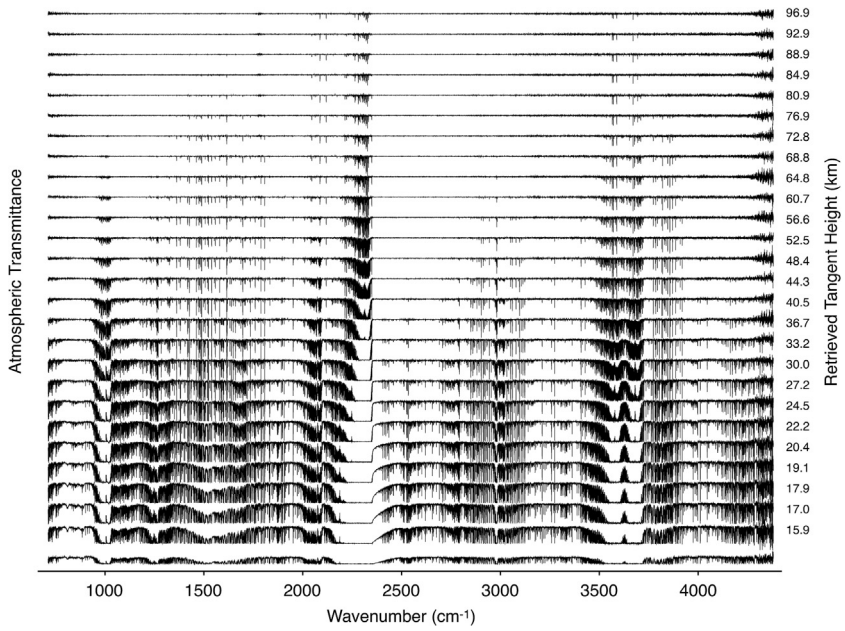

Fig. 7. Typical sequence of spectra for a sunset occultation with the retrieved tangent altitude on the right [1].

part of the processing, retrieved values are interpolated onto the 1 km altitude grid using piecewise quadratic interpolation and are also available on the observed tangent altitude grid. Tangent heights are defined as the altitude at zero path difference of each FTS scan.

To start the level 1 to 2 data processing, *a priori* profiles of pressure and temperature for 0–150 km are generated by combining the values from Environment Canada's operational numerical weather analysis and forecast system Global Environmental Multiscale (GEM) with the predictions of the MSIS (NRL-MSISE-00) model at high altitudes [29]. Optimal Estimation is not used so these values just serve as initial guesses for non-linear squares fitting.

For each occultation, it is necessary as a first step to determine 4 quantities: profiles of the temperature (T), pressure (p) and CO_2 VMR as well as the tangent altitudes (or more precisely the tangent altitude spacing). The spectra provide two independent pieces of information from the relative and absolute intensity of the CO_2 lines. In addition a third quantity can be obtained from the law of hydrostatic equilibrium, $dp/dz = -g(z)\rho(z)$, in which z is altitude, g is the acceleration due to gravity and ρ is the density, together with the ideal gas law to give an equation that couples T, p and z (i.e., given $T(z)$, then $p(z)$ or $z(p)$ can be calculated by integration). The temperature retrievals are based on the relative intensity of CO_2 lines except below 15 km where the GEM values are used and above 125 km where scaled MSIS values are adopted. At high altitudes T and CO_2 VMR are retrieved; pressure is calculated from the law of hydrostatic equilibrium and one reference pressure, CO_2 is retrieved from 65 to 125 km using an empirical function and the relative tangent height spacing is well known from ephemeris. At low altitudes less than about 45 km where refraction is

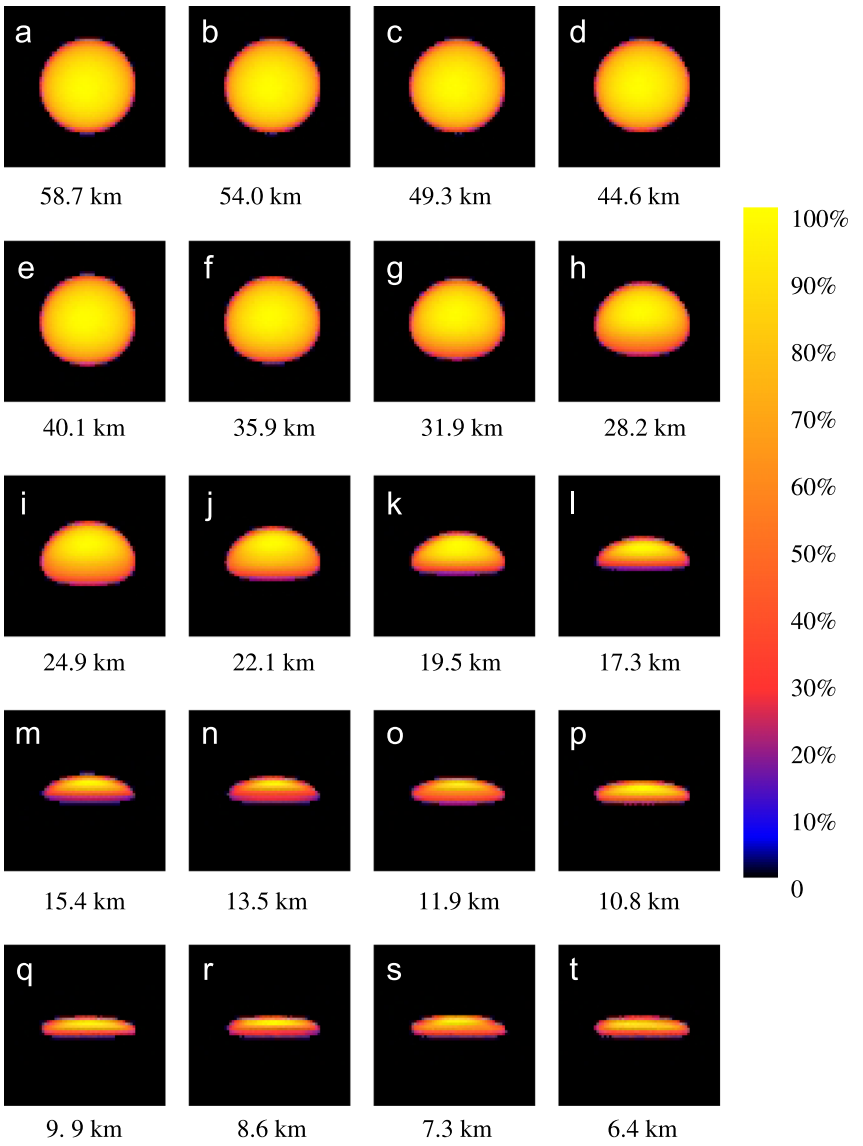

Fig. 8. Sequence of false color solar images from the Visible imager, spaced at 1.5 s intervals for sunset 5909 [27]. The tangent heights listed below each image are interpolated from the FTS and apply to a pixel co-registered with the center of the FTS field of view.

important, T and p are retrieved; a fixed CO_2 VMR is assumed up to 65 km and the tangent height spacing is calculated from the law of hydrostatic equilibrium down to 15 km and $^{18}O^{12}C^{16}O$ is used to generate tangent heights below 15 km. Absolute altitude registration is carried out by comparing the retrieved pressures with the *a priori* values from GEM between 15 and 25 km and shifting the altitudes to achieve the best match.

The second step in the level 1 to 2 data processing is the retrieval of altitude profiles of VMRs of gaseous atmospheric constituents holding T and p fixed. At each tangent altitude, the target VMR is determined along with baseline scaling and slope parameters using the v.3.5 microwindow set. The wavenumber scale of each microwindow is adjusted by cross correlation with the calculated spectrum from the forward model. The VMR profile above the highest analyzed measurement is taken as a constant times the input guess profile. For v.3.5, 37 molecules are retrieved routinely: H_2O, O_3, N_2O, NO, NO_2, HNO_3, N_2O_5, H_2O_2, HO_2NO_2, N_2, O_2, HCl, HF, $ClONO_2$, CFC-11, CFC-12, CFC-113, COF_2, $COCl_2$, COFCl, CF_4, SF_6, CH_3Cl, CCl_4, HCFC-22, HCFC-141b, HCFC-142b, CO, CO_2, CH_4, CH_3OH, H_2CO, HCOOH, C_2H_2, C_2H_6, OCS and HCN as well as 21 of their isotopologues, $H_2{}^{18}O$, $H_2{}^{17}O$, HDO, $O^{13}CO$, $OC^{18}O$, $OC^{17}O$, $O^{13}C^{18}O$, $^{18}OO_2$, $O^{18}OO$, $O^{17}OO$, $N^{15}NO$, ^{15}NNO, $N_2{}^{18}O$, $N_2{}^{17}O$, ^{13}CO, $C^{18}O$, $C^{17}O$, $^{13}CH_4$, CH_3D, $OC^{34}S$ and $O^{13}CS$. Research retrievals are available for ClO, acetone (CH_3COCH_3), PAN (peroxyacetylnitrate, $CH_3COO_2NO_2$) [34], HFC-23 [35] and acetonitrile (CH_3CN) [36]. Many of these research data products will become routine in the next major version (4.0) of the processing, which also will use a more realistic climatology for CO_2 for the T and p retrieval based on G. Toon's model [37] used for Total Carbon Column Observing NetworkTCCON (TCCON).

7.2. Imager processing

The Level 1 data products for the two imagers are a sequence of solar images as illustrated in Fig. 8 for a typical sunset affected by thin clouds [27]. Three pixels from the center of the FTS field of view are used to calculate the atmospheric transmission and are then inverted with the same global fit algorithm used for trace gases to provide the atmospheric extinction in km^{-1} on the standard 1 km altitude grid for both the Visible (525 nm) and Near Infrared (1020 nm) imagers (Level 2).

7.3. MAESTRO processing

The Level 1 data products are optical depth spectra (i.e., $\ln(I_0/I)$) as shown in Fig. 9. MAESTRO processing [7,8] uses T, p and pointing values from ACE-FTS retrievals, although there is a timing offset between ACE and MAESTRO instruments that needs to be corrected for each occultation. The Level 1 to 2 transformation takes place in two steps for version 3.12. The total slant column densities for O_3, NO_2 and aerosols are determined from the optical depths by least-squares fitting. The O_3 absorption cross sections are the GOME flight-model measurements [38] and the NO_2 cross sections are from Vandaele [39]. The slant column densities are then converted to altitude profiles on a 0.5 km altitude grid using a nonlinear

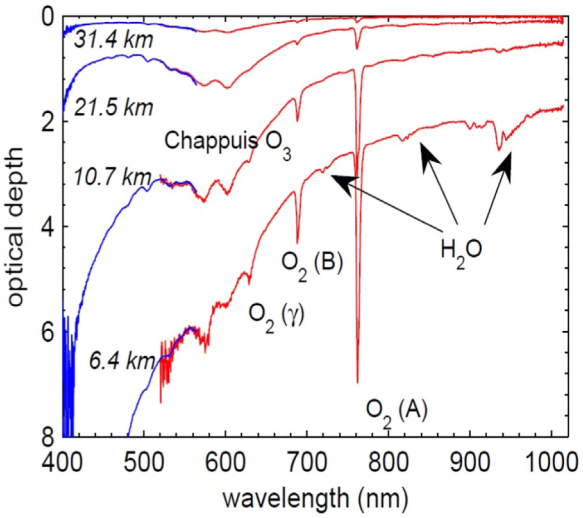

Fig. 9. Typical MAESTRO optical depth spectra [8].

Chahine relaxation inversion. The aerosol extinction profiles are available at 10 wavelengths (525, 530, 560, 603, 675, 779, 875, 922, 995, 1012 nm). MAESTRO also has a H_2O research product [40] derived from the 940 nm overtone band.

8. Validation

After science testing on the ground before launch and a 6-month commission phase between launch and early 2004, routine operations began at the end of February 2004. Some initial validation of selected species such as O_3 was carried out, followed by the main validation of the ACE data products for version 2.2 of the FTS processing. Results were published as a special issue of Atmospheric Chemistry and Physics (⟨http://www.atmos-chem-phys.net/special_issue114.html⟩). Validation papers for 14 "baseline" FTS species, O_3, H_2O, CH_4, N_2O, NO, NO_2, HNO_3, N_2O_5, $ClONO_2$, HCl, HF, CF_3Cl, CF_2Cl_2, CO, plus temperature and aerosol extinction from the imagers were published in 2008 and 2009. Kar et al. [41] validated NO_2 and O_3 from MAESTRO. Overall the ACE data products are verified to be of high quality as discussed in detail in the validation papers. The more recent versions 3.0 and 3.5 show improvements over v.2.2 and their validation is on-going.

ACE data has in turn been widely used to validate data from other satellite instruments, notably MIPAS and MLS (see http://www.ace.uwaterloo.ca/publications.html).

9. Selected science highlights

9.1. Solar and atmospheric atlases

The ACE-FTS routinely records "high Sun" reference spectra with tangent altitudes above 150 km that contain no atmospheric lines. By adding 224,782 individual spectra, an empirical solar atlas has been made covering the 700–4430 cm^{-1} region [42]. Line assignments were made for over 12,000 atomic and molecular lines. The ACE solar

atlas has proved to be useful in astronomy and atmospheric science as a reference spectrum.

Five atlases of the Earth's atmosphere were made for Arctic summer, Arctic winter, mid-latitude summer, mid-latitude winter and the tropics [43]. The spectra cover the 6–126 km altitude range in 4 km intervals (i.e., 31 spectra per atlas). Each atlas was made by adding almost 1000 FTS limb transmission spectra in the 700–4400 cm^{-1} region to improve the signal-to-noise ratio. In addition to digital data, representative plots in pdf format are available at 10 km (troposphere), 30 km (stratosphere), 70 km (mesosphere) and 110 km (lower thermosphere).

The limb geometry of the ACE atlases is the same as the geometry used to record transit spectra of exoplanets [44]. In transit spectra the size of the dip in the light from the parent star is measured as function of wavelength as the planet passes in front of the star. The depth of the dip is related to the effective size of the planet, which is a function of the atmospheric transmission (e.g., if the atmosphere is transparent at a certain wavelength then the dip will be smaller). The ACE atlases are thus similar to the transit spectra expected for Earth-like exoplanets.

9.2. Organic molecules in the troposphere

The emission of organic molecules along with nitrogen oxides is responsible for air pollution. NO and NO_2 act as catalysts for the low-temperature oxidation of volatile organic compounds and lead to the formation of tropospheric ozone as a by-product. ACE-FTS detects a number of organic source gases, the nitrogen oxide catalysts and the resulting ozone in the upper troposphere. For example, the C_1 series of oxygenated molecules CH_3OH [45], CH_2O [46] and HCOOH [47] has been measured at elevated concentrations in biomass burning plumes and at background levels. Methanol is the second most abundant organic molecule in the atmosphere after methane and ACE was able to determine the first global distribution. For hydrocarbons, CH_4, C_2H_2, C_2H_4 and C_2H_6 have all been measured.

ACE organics have been compared with the predictions of a number of chemical transport models including GEOS-Chem [47], LMDz-INCA [45,46], GEM-AQ [48] and WACCM [49]. These chemical transport models can be integrated with numerical weather forecast models to make operational "chemical weather forecasts". Although ACE observations and models are in general agreement, model improvements in terms of chemistry, dynamics and emissions inventories are clearly needed.

9.3. Trends in atmospheric composition

Climate change is driven by increases in the abundances of greenhouse gases such as CO_2, which acts as the "control knob" for the Earth's climate [50]. An assumed fixed CO_2 concentration is used in the ACE-FTS retrievals at low altitudes. At higher altitudes, however, atmospheric refraction becomes negligible and it becomes possible to retrieve routinely the CO_2 VMR and temperature. Emmert et al. [2] found the observed trend for the CO_2 VMR of 23.5 $\pm$ 3.2 ppm/decade at an altitude of 101 km to be nearly twice the value predicted by an NCAR global model. Although the chemistry and dynamics in the upper atmosphere are relatively simple, discrepancies between observations and model predictions likely point to problems with the simulation of vertical transport.

Long-lived chlorine- and bromine-containing gases responsible for ozone depletion in the stratosphere have been banned by the Montreal Protocol. Temporarily CFCs (chlorofluorocarbons) have been replaced by HCFCs (hydrochlorofluorocarbons) that have shorter atmospheric lifetimes, because they react with the OH free radical. HCFCs still destroy stratospheric ozone so they are in turn being replaced by HFCs (hydrofluorocarbons) that contain no chlorine. Halogenated molecules are also very powerful greenhouse gases so the Montreal Protocol has the added benefit of reducing global warming.

Nearly twenty halogen-containing gases have been retrieved from ACE spectra including the main CFC, HCFC and HFC source gases. These species are destroyed by UV photolysis in the stratosphere and lead to the $ClONO_2$, F_2CO, FClCO and Cl_2CO intermediates, and ultimately result in the formation of HCl and HF (all of which are measured by ACE). Trends in halogen-containing gases have been measured using ACE data [3], and Nassar et al. [51,52] and Brown et al. [53] have determined stratospheric fluorine and chlorine budgets. Because of the success of the Montreal Protocol, chlorine-containing gases and HCl are declining, but many fluorine-containing gases and HF are still increasing, but at a slower rate than before [53]. One exception is that HCl is temporarily increasing in the lower stratosphere in the northern hemisphere as a result of a temporary change in atmospheric circulation since 2007 [54]. The age of the air in this region has increased (although climate change predicts a decrease) so there is additional time for photolysis to make the HCl product gas.

9.4. Stratospheric ozone chemistry

The Antarctic "ozone hole" and springtime Arctic ozone declines are caused primarily by the chemical conversion of the inactive chlorine reservoir compounds HCl and $ClONO_2$, which do not react with O_3, to the active ClO radical, catalyzed by polar stratospheric clouds (PSCs). The ACE mission is able to measure all of the main components involved in activated polar chlorine chemistry: O_3, HCl, $ClONO_2$, ClO, HNO_3, H_2O and PSCs. For example, the ACE-FTS measurements of HCl, $ClONO_2$ and ClO were used to study chlorine partitioning during the very cold 2005 Arctic winter and spring [55].

9.5. Asian monsoon

The Asian summer monsoon creates a strong high pressure region (anticyclone) centered over Tibet that confines pollution in the upper troposphere. This enhanced pollution is the result of rapid vertical transport of surface air from China, India and the surrounding region. Park et al. [56] found that the degree of enhancement was inversely related to the atmospheric lifetime as expected for rapid transport of polluted air from the surface. Moreover, primarily stratospheric molecules such as

HCl and O_3 were depleted in the upper troposphere by the rapid flow of air from below. Randel et al. [4] used the HCN tracer to show that the Asian monsoon is uniquely able to inject pollution directly into the stratosphere.

9.6. Atmospheric effects of solar wind

Energetic particles in the solar wind can produce NO in the upper atmosphere. Nitrogen atoms are produced by energetic collisions in the mesosphere and lower thermosphere, which then lead to the formation of NO and NO_2 (NO_x). Usually this NO_x is too high in the atmosphere to react with stratospheric ozone, except during special circumstances. During the dark polar winter, the cold air in the vortex can descend and deposit NO_x in the stratosphere where it can destroy ozone via the NO_x cycle. The effect is enhanced by intense solar storms which can produce NO_x relatively low in the atmosphere or by very cold temperatures which cause unusually strong descent. These effects have been studied using ACE data for NO and NO_2 [57,58]. Global warming causes an increase in surface temperatures but a decrease in temperatures in the upper atmosphere so that this effect could be increasingly significant in the future.

ACE observations led to the discovery that N_2O can be made by energetic particle precipitation [59,60]. N_2O is the most important uncontrolled ozone-depleting substance because long-lived halogenated gases are controlled by the Montreal Protocol [61]. Before the ACE work, it was believed that all atmospheric N_2O originated at the Earth's surface primarily from microbial activity. N_2O has a long atmospheric lifetime but it reacts with $O(^1D)$ atoms in the stratosphere to yield NO. N_2O is the primary source of NO_x in the stratosphere and therefore along with the HO_x and ClO_x chemical cycles controls destruction of ozone. During the polar night N_2O can be created by energetic particle precipitation in the upper mesosphere/lower thermosphere and transported downward to the stratosphere by major sudden stratospheric warming events. The formation of N_2O by auroral activity is therefore a potential new mechanism for the destruction of stratospheric ozone.

9.7. Polar mesospheric clouds

ACE-FTS has recorded the first spectra of polar mesospheric clouds (PMCs or noctilucent clouds), which prove to be small ice particles with ~50 nm effective radius as expected [1]. PMCs form at high latitudes near the mesopause at about 90 km around the time of the summer solstice when the temperatures are very low. Climate change has decreased temperatures in the upper atmosphere and increased the amount of water vapor (from the increase in atmospheric methane) leading to more frequent occurrence of PMCs. Petelina and Zasetsky [62] used the high resolution of the ACE-FTS to infer the ice temperature directly from the shift in the peak position of the ice absorption band at 3 μm.

10. Conclusions

For a small science satellite mission, ACE has been remarkably successful with over 400 ACE-related papers published. Now in its 13th year since launch, the satellite is still working well and we anticipate many more years of science operations. The longevity of ACE makes the data particularly valuable for monitoring changes in atmospheric composition as a function of altitude on a global scale. For example, ACE measures the halogenated gases associated with stratospheric ozone depletion and thus monitors the effectiveness of the Montreal Protocol. Long-lived halogenated gases are also important climate change gases because of their large global warming potentials. Indeed ACE measures all major greenhouse gases and aerosols that drive climate change, and provides data to test and validate climate prediction models. ACE also measures the major organic molecules and nitrogen oxides responsible for air pollution in the troposphere. As "chemical weather forecasting" becomes increasingly sophisticated, ACE provides an extensive data set to test the chemical transport models used to make air pollution predictions.

Acknowledgments

We thank the ACE team of scientists, engineers and managers whose efforts have made the mission a success. Funding for ACE is provided primarily by the Canadian Space Agency. We also are grateful for the launch and continuing support provided by NASA. We thank A. Deepak Publishing, Hampton, VA, USA for permission to reproduce Figs. 1–5, 7–9 from *The Atmospheric Chemistry Experiment ACE at 10: A Solar Occultation Anthology*, P. Bernath (editor, 2013), and R. Hughes for preparing Fig. 6.

References

[1] Bernath PF, McElroy CT, Abrams MC, Boone CB, Butler M, Camy-Peyret C, et al. Atmospheric Chemistry Experiment (ACE): mission overview. Geophys Res Lett, 32; L15S01. http://dx.doi.org/10.1029/2005GL022386 ⟨http://www.ace.uwaterloo.ca/⟩.
[2] Emmert JT, Stevens MH, Bernath PF, Drob DP, Boone CD. Observations of increasing carbon dioxide concentration in Earth's thermosphere. Nat Geosci 2012;5:868–71.
[3] Brown A, Chipperfield MP, Boone C, Wilson C, Walker K, Bernath P. Trends in atmospheric halogen containing gases since 2004. J Quant Spectrosc Radiat Transf 2011;112:2552–66.
[4] Randel WJ, Park M, Emmons L, Kinnison D, Bernath P, Walker KA, et al. Asian monsoon transport of pollution to the stratosphere. Science 2010;328:611–3.
[5] Sioris CE, Zou J, Plummer DA, Boone CD, McElroy CT, Sheese PE, et al. Upper tropospheric water vapour variability at high latitudes: 1. Influence of the annular modes. Atmos Chem Phys 2016;16:3265–78.
[6] Buijs HL, Soucy MA, Lachance R. ACE-FTS hardware and level 1 processing. In: Bernath P, editor. The atmospheric chemistry experiment ACE at 10: a solar occultation anthology. Hampton, VA, USA: A. Deepak Publishing; 2013. p. 53–80.
[7] McElroy CT, Nowlan CR, Drummond JR, Bernath PF, Barton DV, Dufour DG, et al. The ACE-MAESTRO instrument on SCISAT: description, performance and preliminary results. Appl Opt 2007;46:4341–56.
[8] McElroy CT, Barton DV, Nowlan CR, Drummond JR. MAESTRO: The SCISAT UV-Visible-Near IR instrument. In: Bernath P, editor. The

atmospheric chemistry experiment ACE at 10: a solar occultation anthology. Hampton, VA, USA: A. Deepak Publishing; 2013. p. 81–101.
[9] Levelt PF, Hilsenrath E, Leppelmeier GW, van den Oord GHJ, Bhartia PK, Tamminen J, et al. Science Objectives of the Ozone Monitoring Instrument. IEEE Trans Geosci Remote Sensing 2006;44:1199–208.
[10] Beer R, Glavich TA, Rider DM. Tropospheric emission spectrometer for the Earth Observing System's Aura satellite. Appl Opt 2001;40:2356–67.
[11] Bovensmann H, Burrows JP, Buchwitz M, Frerick J, Noël S, Rozanov VV. SCIAMACHY: mission objectives and measurement modes. J Atmos Sci 1999;56:127–50.
[12] Fischer H, Birk M, Blom C, Carli B, Carlotti M, von Clarmann T, et al. MIPAS: an instrument for atmospheric and climate research. Atmos Chem Phys 2008;8:2151–88.
[13] Kyrölä E, Tamminen J, Leppelmeier GW, Sofieva V, Hassinen S, Bertaux JL, et al. GOMOS on Envisat: an overview. Adv Space Res 2004;33:1020–8.
[14] Eriksson P, Merino F, Murtagh D, Baron P, Ricaud P, de la Noë J. Studies for the Odin sub-millimetre radiometer: I. Radiative transfer and instrument simulation. Can J Phys 2002;80:321–40.
[15] Llewellyn EJ, Lloyd ND, Degenstein DA, Gattinger RL, Petelina SV, Bourassa AE, et al. The OSIRIS instrument on the Odin spacecraft. Can J Phys 2004;82:411–22.
[16] Mlynczak MG. Energetics of the mesosphere and lower thermosphere and the SABER experiment. Adv Space Res 1997;20:1177–83.
[17] Gordley LL, Hervig ME, Fish C, Russell III JMR, Bailey S, Cook J, et al. The solar occultation for ice experiment. J Atmos Solar-Terr Phys 2009;71:300–15.
[18] Waters JW, Froidevaux L, Harwood RS, Jarnot RF, Pickett HM, Read WG, et al. The earth observing system microwave limb sounder (EOS MLS) on the Aura Satellite. IEEE Trans Geosci Remote Sensing 2006;44:1075–92.
[19] Rault DF, Loughman RP. The OMPS Limb Profiler environmental data record algorithm theoretical basis document and expected performance. IEEE Trans Geosci Remote Sensing 2013;51:2505–27.
[20] Clerbaux C, Boynard A, Clarisse L, George M, Hadji-Lazaro J, Herbin H, et al. Monitoring of atmospheric composition using the thermal infrared IASI/MetOp sounder. Atmos Chem Phys 2009;9(16):6041–54.
[21] Zoogman P, Liu X, Suleiman RM, Pennington WF, Flittner DE, Al-Saadi JA, et al. Tropospheric Emissions: Monitoring of Pollution (TEMPO). J Quant Spectrosc Radiat Transf 2016 (this issue).
[22] Veefkind J, Aben I, McMullan K, Förster H, de Vries J, Otter G, et al. TROPOMI on the ESA (Sentinel-5) precursor: a GMES mission for global observations of the atmospheric composition for climate, air quality and ozone layer applications, the Sentinel missions – new opportunities for science. Remote Sens Environ 2012;120:70–83.
[23] Gunson MR, Abbas MM, Abrams MC, Allen M, Brown LR, Brown TL, et al. The Atmospheric Trace Molecule Spectroscopy (ATMOS) Experiment: deployment on the ATLAS Space Shuttle missions. Geophys Res Lett, 23; 2333–6.
[24] Kent GS, Winker DM, Osborn MT, Skeens KM. A model for the separation of cloud and aerosol in SAGE II occultation data. J Geophys Res 1993;98:20725–35.
[25] Kuze A, Suto H, Nakajima M, Hamazaki T. Thermal and near infrared sensor for carbon observation Fourier-transform spectrometer on the Greenhouse Gases Observing Satellite for greenhouse gases monitoring. Appl Opt 2009;48:6716–33.
[26] Gilbert KL, Turnbull DN, Walker KA, Boone CD, McLeod SD, Butler M, et al. The onboard imagers for the Canadian ACE SCISAT-1 mission. J Geophys Res 2007;112:D12207.
[27] Gilbert KL. The ACE imagers. In: Bernath P, editor. The Atmospheric Chemistry Experiment ACE at 10: A Solar Occultation Anthology. Hampton, VA, USA: A. Deepak Publishing; 2013. p. 129–38.
[28] Walkty I, Kohut K. SCISAT-1 spacecraft. In: Bernath P, editor. The Atmospheric Chemistry Experiment ACE at 10: A Solar Occultation Anthology. Hampton, VA, USA: A. Deepak Publishing; 2013. p. 43–52.
[29] Boone CD, Nassar R, Walker KA, Rochon Y, McLeod SD, Rinsland CP, et al. Retrievals for the Atmospheric Chemistry Experiment Fourier Transform Spectrometer. Appl Opt 2005;44:7218–31.
[30] Boone CD, Walker KA, Bernath PF. Version 3 Retrievals for the Atmospheric Chemistry Experiment Fourier Transform Spectrometer (ACE-FTS). In: Bernath P, editor. The Atmospheric Chemistry Experiment ACE at 10: A Solar Occultation Anthology. Hampton, VA, USA: A. Deepak Publishing; 2013. p. 103–27.
[31] Carlotti M. Global-fit approach to the analysis of limb-scanning atmospheric measurements. Appl Opt 1988;27:3250–4.
[32] Bernath PF. Spectra of Atoms and Molecules. 3rd edNew York: Oxford University Press; 2016.
[33] Rothman LS, Jacquemart D, Barbe A, Benner DC, Birk M, Brown LR, et al. The HITRAN 2004 molecular spectroscopic database. J Quant Spectrosc Rad Transfer 2005;96:139–204.
[34] Tereszchuk KA, Moore DP, Harrison JJ, Boone CD, Park M, Remedios JJ, et al. Observations of peroxyacetyl nitrate (PAN) in the upper troposphere by the Atmospheric Chemistry Experiment – Fourier Transform Spectrometer (ACE-FTS). Atmos Chem Phys 2013;13:5601–13.
[35] Harrison JJ, Boone CD, Brown AT, Allen NDC, Toon GC, Bernath PF. First remote-sensing observations of trifluoromethane (HFC-23) in the upper troposphere and lower stratosphere. J Geophys Res 2012;117:D05308.
[36] Harrison JJ, Bernath PF. ACE-FTS Observations of acetonitrile in the lower stratosphere. Atmos Chem Phys 2013;13:7405–13.
[37] Wunch D, Toon GC, Wennberg PO, Wofsy SC, Stephens BB, Fischer ML, et al. Calibration of the Total Carbon Column Observing Network using aircraft profile data. Atmos Meas Tech 2010;2010(3):1351–62.
[38] Burrows JP, Richter A, Dehn A, Deters B, Himmelmann S, Voigt S, et al. Atmospheric remote-sensing reference data from GOME-2. Temperature-Dependent Absorption Cross Sections of O_3 in the 231–794 nm Range. J Quant Spectrosc Rad Transfer 1999;61:509–17.
[39] Hermans C, Vandaele AC, Carleer M, Fally S, Colin R, Jenouvrier A, et al. Absorption cross-sections of atmospheric constituents: NO_2, O_2, and H_2O. Environ Sci Pollut Res 1999;6:151–8.
[40] Sioris CE, Zou J, McElroy CT, McLinden CA, Vömel H. High vertical resolution water vapour profiles in the upper troposphere and lower stratosphere retrieved from MAESTRO solar occultation spectra. Adv Space Res 2010;46:642–50.
[41] Kar J, McElroy CT, Drummond JR, Zou J, Nichitiu F, Walker KA, et al. Initial comparison of ozone and NO_2 profiles from ACE-MAESTRO with balloon and satellite data. J Geophys Res 2007;112:D16301.
[42] Hase F, Wallace L, McLeod SD, Harrison JJ, Bernath PF. The ACE-FTS atlas of the infrared solar spectrum. J Quant Spectrosc Rad Transfer 2010;111:521–8.
[43] Hughes R, Bernath P, Boone C. ACE infrared spectral atlases of the earth's atmosphere. J Quant Spectrosc Rad Transfer 2014;148:18–21.
[44] Bernath PF. Molecular opacities for exoplanets. Philos Trans R Soc A 2014;372:20130087.
[45] Dufour G, Szopa S, Hauglustaine DA, Boone CD, Rinsland CP, Bernath PF. The influence of biogenic emissions on upper tropospheric methanol as revealed from space. Atmos Chem Phys 2007;7:6119–29.
[46] Dufour G, Szopa S, Barkley MP, Boone CD, Perrin A, Palmer PI, et al. Global upper-tropospheric formaldehyde: seasonal cycles observed by the ACE-FTS satellite instrument. Atmos Chem Phys 2009;9:3893–910.
[47] Abad GG, Bernath PF, Boone CD, McLeod SD, Manney GL, Toon GC. Global distribution of upper tropospheric formic acid from the ACE-FTS. Atmos Chem Phys 2009;9:8039–47.
[48] Lupu A, Kaminski JW, Neary L, McConnell JC, Toyota K, Rinsland CP, et al. Hydrogen cyanide in the upper troposphere. Atmos Chem Phys 2009;9:4301–13.
[49] Park M, Randel WJ, Kinnison DE, Emmons LK, Bernath PF, Walker KA, et al. Hydrocarbons in the upper troposphere and lower stratosphere observed from ACE-FTS and comparisons with WACCM. J Geophys Res 2013;118:1–17.
[50] Lacis AA, Schmidt GA, Rind D, Reto A, Ruedy RA. Atmospheric CO_2: principal control knob governing earth's temperature. Science 2010;330:356–9.
[51] Nassar R, Bernath PF, Boone CD, Clerbaux C, Coheur PF, Dufour G, et al. A global inventory of stratospheric chlorine in 2004. J Geophys Res 2006;111:D22312.
[52] Nassar R, Bernath PF, Boone CD, McLeod SD, Skelton R, Walker KA, et al. A global inventory of stratospheric fluorine in 2004 based on Atmospheric Chemistry Experiment Fourier transform spectrometer (ACE-FTS) measurements. J Geophys Res 2006;111:D22313.
[53] Brown AT, Chipperfield MP, Richards NAD, Boone C, Bernath PF. Global stratospheric fluorine inventories for 2004–2009 from Atmospheric Chemistry Experiment Fourier Transform Spectrometer (ACE-FTS) measurements. Atmos Chem Phys 2014;14:267–82.
[54] Mahieu E, Chipperfield MP, Notholt J, Anderson J, Bernath PF, Blumenstock T, et al. Recent northern hemisphere hydrogen chloride increase due to atmospheric circulation change. Nature 2014;515:104–7.
[55] Dufour G, Nassar R, Boone CD, Skelton R, Walker KA, Bernath PF, et al. Partitioning between the inorganic chlorine reservoirs HCl

and $ClONO_2$ during the Arctic winter 2005 from the ACE-FTS. Atmos Chem Phys 2006;6:2355–66.
[56] Park M, Randel WJ, Emmons LK, Bernath PF, Walker KA, Boone CD. Chemical Isolation in the Asian Monsoon Anticyclone observed in Atmospheric Chemistry Experiment (ACE-FTS) data. Atmos Chem Phys 2008;8:757–64.
[57] Randall CE, Harvey VL, Singleton CS, Bernath PF, Boone CD, Kozyra JU. Enhanced NO_x in 2006 linked to strong upper stratospheric Arctic vortex. Geophys Res Lett 2006;33:L18811.
[58] Randall CE, Harvey VL, Siskind DE, France J, Bernath PF, Boone CD, et al. NO_x descent in the Arctic middle atmosphere in early 2009. Geophys Res Lett 2009;36:L18811.
[59] Semeniuk K, McConnell JC, Jin JJ, Jarosz JR, Boone CD, Bernath PF. N_2O production by high energy auroral electron precipitation. J Geophys Res 2008;113:D16302.
[60] Sheese PE, Walker KA, Boone CD, Bernath PF, Funke B. Nitrous oxide in the atmosphere: First measurements of a lower thermospheric source. Geophys Res Lett 2016:43. http://dx.doi.org/10.1002/2015GL067353.
[61] Ravishankara AR, Daniel JS, Portmann RW. Nitrous oxide (N_2O): the dominant ozone-depleting substance emitted in the 21st century. Science 2009;326:123–5.
[62] Petelina SV, Zasetsky AY. Temperature of mesospheric ice retrieved from the O-H stretch band. Geophys Res Lett 2009;36:L15804.